

# QUANTITATIVE SCINTILLATION SCREEN STUDIES AT GSI-LINAC AND RELATED MODEL CALCULATIONS

E. Gütlich\*, P. Forck, B. Walasek-Höhne, GSI, Darmstadt, Germany  
 W. Ensinger, Technical University of Darmstadt, Darmstadt, Germany

## Abstract

Scintillation screens are commonly used at accelerator facilities, however their imaging qualities are not well understood, especially for high current ion beam operation. Several types of inorganic scintillators were investigated for various ion species and energies of 4.8 and 11.4 MeV/u. To validate the imaging quality of the scintillators a scraper scan method was established. Some of the investigated materials show dependence on the ion energy.  $Al_2O_3$  showed the best results. For 4.8 MeV/u the obtained beam profile is in good agreement with the reference methods, while for 11.4 MeV/u the screen image does not reflect the beam distribution. For  $Al_2O_3$  a model is under development, which takes the radial dose distribution of the ions and thus an overlap of the tracks into account. For  $Al_2O_3$  the model is able to describe the observed effects and reconstruct saturated images. Spectroscopic investigations were performed, to determine the influence of the ion beam intensity on luminescence spectra of the materials. No significant dependence was found.

## INTRODUCTION

Scintillation screens are widely used for beam alignment and beam profile measurement in nearly all accelerator facilities. Moreover, these screens are an essential part of a pepper-pot emittance system. The interest of pepper-pot emittance measurements arises from the two dimensional phase space information which is obtained out of one macro pulse. Compared to normal slit grid method it also reduces the time of beam interruption by 1-2 orders of magnitude [1]. However, there had been doubts concerning the accuracy of the pepper-pot method [2], which might be related to a possible image deformation by the scintillating screen as reported in [3, 4].

The imaging properties of the materials in Table 1 were investigated with ion beams of  $Ar^{10+}$  and  $^{48}Ca^{10+}$  at energies of 4.8 and 11.4 MeV/u and different beam currents as delivered by the LINAC. The typical size of the ion beam was  $\sigma = 2$  mm. The image of the beam spot was projected to the horizontal and vertical plane of the beam. For the characterization of the distribution  $p_i(x_i)$  not only the center  $\mu$  (1st moment) and standard deviation  $\sigma$  (2nd moment) were used, but also the skewness  $\gamma$  (prop. to 3rd moment, parameter of the asymmetry) and the kurtosis  $\kappa$  (prop. to 4th moment, the peakedness) [5].

\* E-Mail: e.guetlich@gsi.de

Table 1: Compilation of Investigated Materials

Type	Material	Supplier
Ceramic	$ZrO_2 : Y$ (Z700),	BCE Special Ceramics
	$ZrO_2 : Y + 20\% Al_2O_3$	
	(Z700-20A),	
	$ZrO_2 : Mg$ (Z507),	
	$AlN, Al_2O_3,$	
	$Al_2O_3 : Cr,$	
Quartz glass	Quartz ( <i>Herasil</i> 102),	Heraeus

## SCREEN INVESTIGATION

An example for high current measurement is shown in Fig.1 where the screens were irradiated by  $Ar^{10+}$  at 11.4 MeV/u with a current of 260  $\mu A$  within 200  $\mu s$  delivery time corresponding to  $3.3 \cdot 10^{10}$  particles per pulse (ppp). The peak power was 12 kW while the average power was 4.1 W. All materials were mounted on one target ladder and were investigated within 2 hours to ensure same beam parameters for the materials. As expected the light yield of the various materials differs by several orders of magnitude. For  $AlN$  and  $Al_2O_3$  the light yield and statistical moments are relatively stable, while for the other materials the observed variations are bigger. The determined beam width varies within a factor of two and the higher moments even show a more complex behavior. The chromatic aberration of the optics and signal intensity on the CCD-Chip contribute only an error of about 1% to the calculated beam width. This measurement clearly shows that the different materials represent different beam parameters for the same ion beam.

## COMPARISON WITH REFERENCE METHODS

To determine the imaging qualities of the screens, different profile measurement methods have been compared. To obtain a better resolution compared to SEM-Grid, a scraper scan method was established. The scraper is scanning through the ion beam. All ions that hit the scraper are completely stopped in the material. For each position of the scraper, the beam current behind the scraper is measured via a current transformer (about 20 points/mm). By calculating the first numerical derivative of the current signal, one obtains the beam profile with a good resolution. In Fig. 2 the beam profiles are compared for  $^{48}Ca^{10+}$  at 4.8 MeV/u and  $4.3 \cdot 10^{10}$  ppp within 5 ms beam delivery time.

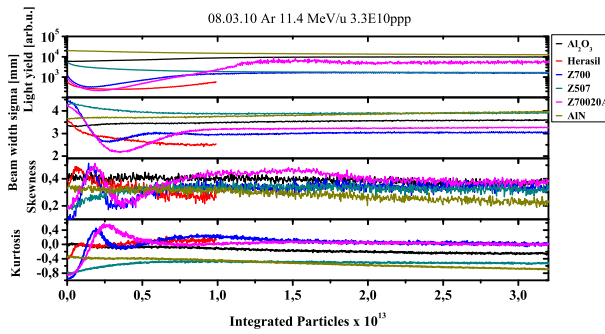


Figure 1: Light yield, beam width, Skewness and Kurtosis over the integrated number of particles. Each point in the curves represent the specific value for one macro pulse. Beam parameters:  $Ar^{10+}$  @ 11.4 MeV/u,  $3.3 \times 10^{10}$  ppp, 260  $\mu A$ , 200  $\mu s$ , 1.7 Hz, 1000 pulses,  $P_{peak} = 12$  kW,  $P_{aver} = 4.1$  W

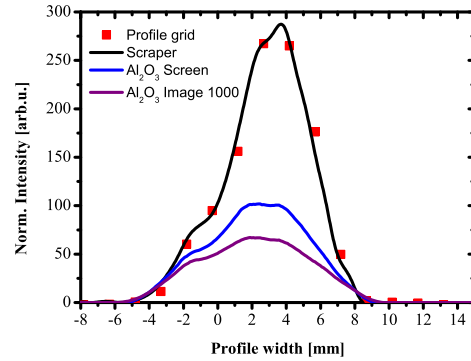


Figure 3: Comparison of reference methods with profiles obtained by  $Al_2O_3$  screen (1<sup>st</sup> and 1000<sup>th</sup> macro pulse). Beam parameters:  $^{48}Ca^{10+}$  @ 11.4 MeV/u,  $1.87 \times 10^{10}$  ppp, 26  $\mu A$ , 1.2 ms, 1 Hz,  $P_{peak} = 1.37$  kW,  $P_{aver} = 1.63$  W

## SPECTROSCOPIC STUDIES

To understand the mechanisms within a scintillating material, a advanced experimental setup for the spectroscopic investigations has been developed. The setup allows to investigate the spectrum of the material with one additional spacial axis. The investigated strip of the beamspot has a typical width of 1mm depending on the slit setting of the spectrometer. The setup allows to distinguish between the spectrum of the beam center and the outer region, which gives fundamental information about the scintillation process. The spectroscopic studies on the scintillation screens were performed with the Jobin Yvon Horiba CP140-202 spectrograph [6] and a cooled CCD camera (PCO 1600). The spectra are not intensity corrected and normalized to the maximum.

In Fig. 4 the spectra of  $Al_2O_3$  are shown for a  $^{48}Ca^{10+}$  ion beam at 4.8 MeV/u and  $5.4 \times 10^{10}$  ppp within 3.3 ms beam delivery time. The first row shows the spectra of the first macro pulse. One can see that there is no difference the between the spectrum of the center and the outer region of the beamspot. In the second row the spectra of the 100<sup>th</sup> macro pulse are shown. Between 370 and 440 nm the spectra of the center and the outer region of the beamspot are slightly different. Since the efficiency of the optical setup for standard profile measurements is negligible below 370 nm, a difference in the spectra over the beamspot can lead to an incorrect representation of the intensity distribution on the CCD-Chip. The third row shows the temperature behavior of the emission spectrum of  $Al_2O_3$ . One can note that the part of the emission around 400 nm is not as temperature sensitive as the part at 340 nm. The last row shows the spectra recorded right after the macro pulse with an integration time as long as the macro pulse (3.3 ms). It is clear to see that over time the region around 420 nm is more stable then the region around 340 nm.

In Fig. 5 the “partial” beam profiles are shown for different wavelength which can be obtained out of the spec-

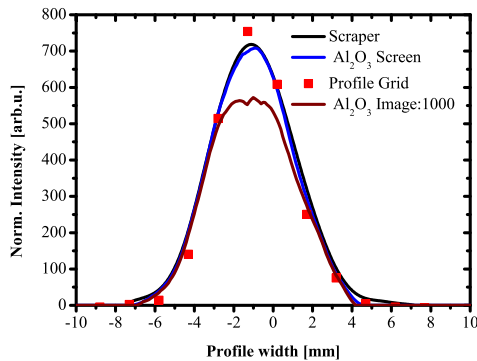


Figure 2: Comparison of reference methods with profiles obtained by  $Al_2O_3$  screen (1<sup>st</sup> and 1000<sup>th</sup> macro pulse). Beam parameters:  $^{48}Ca^{10+}$  @ 4.8 MeV/u,  $4.3 \times 10^{10}$  ppp, 13.5  $\mu A$ , 5 ms, 1 Hz,  $P_{peak} = 317$  W,  $P_{aver} = 1.59$  W

For the first macro pulse the methods are in good agreement, while for the 1000<sup>th</sup> macro pulse a deformation of the profile obtained by the  $Al_2O_3$  screen can be observed. The deformation compared to the other methods can be attributed to both material degradation and spectral effects which will be discussed in the next section. In the case of material degradation it is possible that generated electron- and hole-traps reduce the luminescence efficiency.

In Fig. 3 the same measurement methods are compared again for a  $^{48}Ca^{10+}$  beam on  $Al_2O_3$  screen but with a beam energy of 11.4 MeV/u. The number of particles per pulse has been reduced to keep the deposited energy in the screen constant. The beam profile obtained by the screen does not reflect the same intensity distribution as the reference methods, even for the first macro pulse. The mismatch can not be explained by immediate screen degradation.

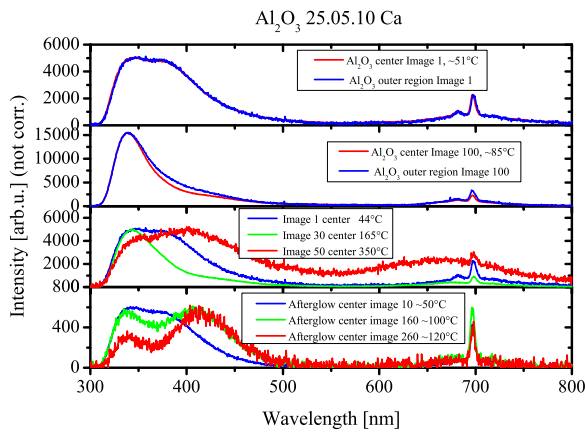


Figure 4: Spectra of  $Al_2O_3$ , within and after the macro pulse, see text. Beam parameters:  $^{48}Ca^{10+}$  @ 4.8 MeV/u,  $5.4 \cdot 10^{10}$  ppp,  $31 \mu A$ , 3.3 ms, 1 Hz,  $P_{peak} = 604$  W,  $P_{aver} = 1.99$  W

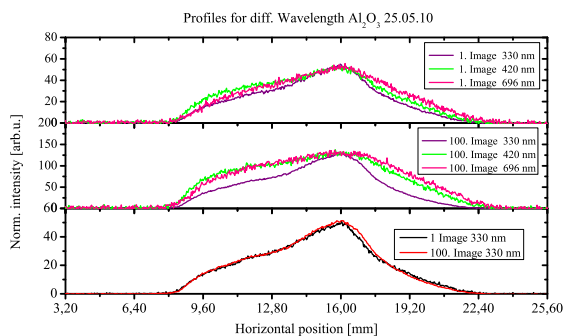


Figure 5: “Partial” beam profiles out of the spectroscopic data (Fig. 4) for different wavelength, see text. Beam parameters see Fig.4

troscopic data shown in Fig. 4. The profiles are integrated over  $\pm 3$  nm around the given wavelength. In the first row the profiles of the first macro pulse are shown for 340 nm ( $F^+$ -Emission), 420 nm ( $F^0$ -Emission) and 696 nm ( $C_7^{3+}$ -Emission). Different profiles are recorded for each wavelength. The second row shows the profiles of the 100<sup>th</sup> macro pulse. The profiles for 696 and 420 nm are comparable only the 340 nm profile is different from the other two. The third row compares the profiles for 340 nm of the first and the 100<sup>th</sup> macro pulse. Only small changes can be observed. This shows that imaging quality of the  $F^+$ -Emission (340 nm) is more stable over time, therefore profile measurements around 340 nm can lead to better results than in the optical region of the spectrum.

### A QUANTITATIVE MODEL FOR ALUMINUM OXIDE

To explain the saturation behavior of  $Al_2O_3$  shown in Fig. 3 a model is under development taking into account the overlap of the ion excitation tracks in space and time.

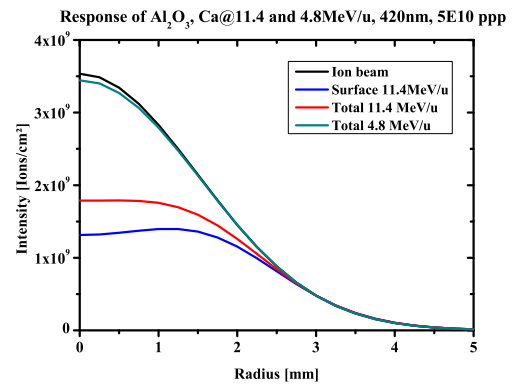


Figure 6: Calculated response of  $Al_2O_3$  Screen

It is based the radial dose distribution of the ions, estimations concerning the behavior in the overlapping regions and a maximal energy dose which can be converted inside the material. In Fig. 6 the calculated response of an  $Al_2O_3$  screen to a Gaussian shaped ion beam with  $5 \cdot 10^{10}$  ppp is shown. The intensity distribution of the ion beam is depicted in black. The response for 4.8 MeV/u ions (light blue) is less effected compared to the response for 11.4 MeV/u ions (red). For comparison only the response of the surface for 11.4 MeV/u is shown in blue without the Lambert-Beer weighted signal from deeper layers. The Difference between 4.8 and 11.4 MeV/u is due to the radial does distribution of the ions which is more influenced by the ion velocity then by the stopping power. The developed model is able to explain the saturation effect in  $Al_2O_3$  and is able to reconstruct saturated images like Fig. 3. Additional experiments are needed with a known beam flux to determine the maximal energy dose.

### REFERENCES

- [1] T. Hoffmann et al., Proc. Beam Instrum. Workshop, Stanford, USA: p.432, (2000).
- [2] J. Pfister et al., Proc. EPAC 2008, Genoa, Italy: p.3449, (2008) and W. Barth, L. Groening, D. Liakin, Proc. DIPAC03 Mainz, p.56 (2003).
- [3] E. Gütlich et al., GSI-Scientific Report 2007-2010, p.105(2007)/p. 126(2008)/p. 143(2009)/to be published (2010), (2007-2008).
- [4] E. Gütlich et al., Scintillation screen investigations for high current ion beams, IEEE TNS Vol. 57, No. 3., pp. 1414 (2010).
- [5] W. H. Press et al., Numerical Recipes 3rd.Edition, Cambridge University Press, New York, p.724 (2007)
- [6] Homepage of Horiba Scientific, <http://www.horiba.com>.